Taylor & Francis
Taylor & Francis Group

Journal of Computational and Theoretical Transport

ISSN: 2332-4309 (Print) 2332-4325 (Online) Journal homepage: https://www.tandfonline.com/loi/ltty21

Energy Dependent Source Reconstructions via Explicit Formulations of the Adjoint Particles Flux

C. B. Pazinatto & L. B. Barichello

To cite this article: C. B. Pazinatto & L. B. Barichello (2018) Energy Dependent Source Reconstructions via Explicit Formulations of the Adjoint Particles Flux, Journal of Computational and Theoretical Transport, 47:1-3, 58-83, DOI: 10.1080/23324309.2018.1481432

To link to this article: https://doi.org/10.1080/23324309.2018.1481432

JOURNAL OF COMPUTATIONAL AND THEORETICAL TRANSPORT
2018, VOL. 47, NO. 1–3, 58–83
https://doi.org/10.1080/23324309.2018.1481432

Taylor & Francis
Taylor & Francis Group

Energy Dependent Source Reconstructions via Explicit Formulations of the Adjoint Particles Flux

C. B. Pazinatto[a] and L. B. Barichello[b]

[a]Programa de Pós-graduação em Matemática Aplicada, Universidade Federal do Rio Grande do Sul, Porto Alegre, Rio Grande do Sul, Brazil; [b]Instituto de Matemática e Estatística, Universidade Federal do Rio Grande do Sul, Porto Alegre, Rio Grande do Sul, Brazil

ABSTRACT

An analytical solution to the discrete ordinates approximation of the adjoint to the multigroup transport equation in one-dimensional slab geometry is developed in this work, in order to be used in source estimation problems. The solution is firstly tested in a source-detector problem, where explicit expressions are derived to approximate the absorption rate of particles of internal detectors. Noisy data generated from readings of internal detectors were then used, along with the adjoint formulation, in an iterative process to solve an energy-dependent inverse problem of source reconstruction in the cases of polynomials and piecewise constant sources. The approach is shown to be fast and accurate.

KEYWORDS

Adjoint transport equation; analytical methods; inverse problems; source-detector; source estimation; ADO method

1. Introduction

The adjoint to the transport operator is an important mathematical tool that may be very helpful in the solution of several problems in transport theory, for instance, in nuclear reactor analysis (Duderstadt and Martin 1979), nuclear material detection (Miller and Charlton 2007; Somasundaram and Palmer 2016), nondestructive material identification (Gao and Zhao 2010; Dorn 2000; Kauati, Silva Neto, and Roberty 2001; Haltmeier, Neumann, and Rabanser 2015) and oil well logging (Badruzzaman 1991).

Some of these applications are, in fact, characterized as inverse problems, where the solution of the adjoint transport equation is frequently part of an iterative (optimization) process (Miller and Charlton 2007; Gao and Zhao 2010; Bledsoe and Favorite 2007; Hykes and Azmy 2011). Such approaches may demand relevant computational time and, in this context, fast solutions may be very helpful. In source estimation problems either internal or boundary information are considered known and the

CONTACT L. B. Barichello lbaric@mat.ufrgs.br Instituto de Matemática e Estatística, Universidade Federal do Rio Grande do Sul, Av Bento Goncalves 9500, P.O. Box 15080, Porto Alegre 91509900, Rio Grande do Sul, Brazil.

reconstruction procedure may be related to the definition of some coefficients (parameters) of a proposed basis function expansion (Miller and Charlton 2007; Gao and Zhao 2010; Kauati, Silva Neto, and Roberty 2001; Siewert 1993a).

In this context, given that the *Analytical Discrete Ordinates* (ADO) method (Barichello and Siewert 1999a) has shown to be fast, accurate, and easily implementable for solving many problems related to transport calculations (Barichello and Siewert 1999b; Siewert 2000; Scherer, Prolo Filho, and Barichello 2009), such a formulation was used to solve monoenergetic adjoint transport problems (Pazinatto, Barros, and Barichello 2016), with a successful application in source estimation (Pazinatto and Barichello 2017).

In this work, we present an extension of the monoenergetic adjoint ADO formulation for the multigroup discrete ordinates model of the adjoint transport equation in slab geometry. We consider heterogeneous media with arbitrary anisotropic scattering and reflective boundary conditions, natural steps to enhance the model in order to handle more practical applications related to inverse problems of source estimation. We first test the adjoint ADO formulation in source-detector evaluations. After that, we use the adjoint solution in an iterative process of energy-dependent source estimation.

In this way, we organize this paper such that in Section 2 we present the forward transport problem of interest, as well as the adjoint operator; in Section 3, we develop the adjoint ADO solution for the proposed problem; continuing, in Section 4, we test the ADO formulation using a source-detector test problem; then, in Section 5, we present two energy-dependent source estimation test problems, for the cases of polynomials and piecewise constant sources; finally, in Section 6, we discuss concluding points and ongoing projects.

2. Mathematical formulation

Let us consider a multilayer slab of thickness Z, composed of R contiguous regions,

$$[0, Z] = \bigcup_{k=1}^{R} [z_{k-1}, z_k]. \tag{1}$$

If, for a fixed k, $1 \leq k \leq R$, a particle detector with absorption cross section $\boldsymbol{\sigma_d} : [0, Z] \rightarrow \mathbb{R}_+^G$ given by

$$\boldsymbol{\sigma_d}(z) = \begin{cases} \boldsymbol{\sigma_d}, & z \in [z_a, z_b] \subseteq [z_{k-1}, z_k], \\ \mathbf{0}, & \text{otherwise}, \end{cases} \tag{2}$$

is placed within region k, then, we can write the absorption rate of particles migrating in all directions within the segment $[z_a, z_b]$, with energy spectrum

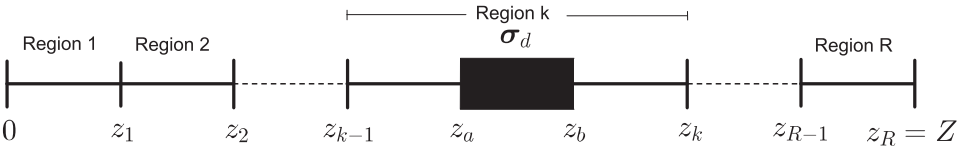

Figure 1. Internal detector.

divided into G energy groups, as

$$r = \langle \boldsymbol{\sigma_d}, \boldsymbol{\psi} \rangle, \tag{3}$$

where we define the inner product (Somasundaram and Palmer 2016)

$$\langle \boldsymbol{h}_1, \boldsymbol{h}_2 \rangle = \sum_{g=1}^{G} \int_{-1}^{1} \int_{0}^{Z} h_{1,g}(z,\mu) h_{2,g}(z,\mu) dz d\mu, \tag{4}$$

for $\boldsymbol{h}_1, \boldsymbol{h}_2 : [0, Z] \times [-1, 1] \to \mathbb{R}^G$. Figure 1 illustrates the location of the detector within the slab.

In Equation (3), $\boldsymbol{\psi} : [0, Z] \times [-1, 1] \to \mathbb{R}^G$ represents the angular flux of particles within the slab, the solution of the transport problem. This way, we define the (forward) transport problem as (Siewert 2000)

$$\mathcal{L}\boldsymbol{\psi} = \boldsymbol{q}, \tag{5a}$$

for $z \in (0, Z)$ the spatial variable and $\mu \in [-1, 1]$ the direction cosine (as measured from the positive z axis), subject to boundary conditions given by

$$\boldsymbol{\psi}(0, \mu) = \boldsymbol{f}_1(\mu) + \alpha_1 \boldsymbol{\psi}(0, -\mu), \tag{5b}$$

$$\boldsymbol{\psi}(Z, -\mu) = \boldsymbol{f}_2(\mu) + \alpha_2 \boldsymbol{\psi}(Z, \mu), \tag{5c}$$

for $\mu \in (0, 1]$, and continuity conditions at the shared interfaces between regions

$$\lim_{z \to z_k^-} \boldsymbol{\psi}(z, \mu) = \lim_{z \to z_k^+} \boldsymbol{\psi}(z, \mu), \tag{5d}$$

for $z \in [0, Z]$ and $\mu \in [-1, 1]$. Here $\mathcal{L}$ is the (forward) transport operator, such that

$$\mathcal{L}\boldsymbol{\psi} = \mu \frac{\partial}{\partial z} \boldsymbol{\psi}(z, \mu) + \boldsymbol{S}\boldsymbol{\psi}(z, \mu) - \frac{1}{2} \sum_{l=0}^{\mathrm{L}} P_l(\mu) \boldsymbol{T}_l \int_{-1}^{1} P_l(\mu') \boldsymbol{\psi}(z, \mu') d\mu'. \tag{5e}$$

In this work, for $z \in [z_{k-1}, z_k]$, we write $\boldsymbol{S} = \boldsymbol{S}_k$, where $\boldsymbol{S}_k \in \mathbb{R}^{G \times G}$ is a diagonal matrix whose entries are the total macroscopic cross section of each energy group. For a fixed integer $L \geq 0$ and $0 \leq l \leq L$, $\boldsymbol{T}_l = \boldsymbol{T}_{l,k}$, where $\boldsymbol{T}_{l,k} \in \mathbb{R}^{G \times G}$ is a matrix representing the transfer cross sections between energy groups, and P_l is the l-th order Legendre polynomial. Finally, $\boldsymbol{f}_1, \boldsymbol{f}_2 : [0, 1] \to \mathbb{R}_+^G$ represent the flux of incoming particles at the

boundaries of the slab, $\alpha_1, \alpha_2 \in [0,1]$ are specular reflection coefficients, and $\boldsymbol{q} = \boldsymbol{q}_k$, $\boldsymbol{q}_k : [z_{k-1}, z_k] \times [-1,1] \to \mathbb{R}^G$ is an internal source of particles.

When computing the absorption rate, Equation (3), of a fixed particle detector, for each source $\boldsymbol{q}$ a new evaluation is required of the transport problem in Equations (5a–5e). We can avoid such inconvenience if we use an alternative expression to evaluate the absorption rate that, in fact, depends explicitly on $\boldsymbol{q}$. Thus, we rewrite Equation (3) in terms of the adjoint angular flux $\boldsymbol{\psi}^\dagger$,

$$r = \langle \boldsymbol{\psi}^\dagger, \boldsymbol{q} \rangle - P[\boldsymbol{\psi}, \boldsymbol{\psi}^\dagger] \tag{6}$$

where $\boldsymbol{\psi}^\dagger : [0, Z] \times [-1,1] \to \mathbb{R}^G$ is the solution of the adjoint transport problem

$$\mathcal{L}^\dagger \boldsymbol{\psi}^\dagger = \boldsymbol{\sigma_d}, \tag{7a}$$

for $z \in (0, Z) \times [-1,1]$, subject to boundary conditions given by

$$\boldsymbol{\psi}^\dagger(0, -\mu) = \alpha_1 \boldsymbol{\psi}^\dagger(0, \mu), \tag{7b}$$

$$\boldsymbol{\psi}^\dagger(Z, \mu) = \alpha_2 \boldsymbol{\psi}^\dagger(Z, -\mu), \tag{7c}$$

for $\mu \in (0,1]$, and interface conditions

$$\lim_{z \to z_k^-} \boldsymbol{\psi}^\dagger(z, \mu) = \lim_{z \to z_k^+} \boldsymbol{\psi}^\dagger(z, \mu), \tag{7d}$$

for $z \in [0, Z]$ and $\mu \in [-1,1]$. We define $\mathcal{L}^\dagger$, the adjoint (or backward) transport operator, such that

$$\mathcal{L}^\dagger \boldsymbol{\psi}^\dagger = -\mu \frac{\partial}{\partial z} \boldsymbol{\psi}^\dagger(z, \mu) + \boldsymbol{S} \boldsymbol{\psi}^\dagger(z, \mu) - \frac{1}{2} \sum_{l=0}^{L} P_l(\mu) \boldsymbol{T}_l^T \int_{-1}^{1} P_l(\mu') \boldsymbol{\psi}^\dagger(z, \mu') d\mu', \tag{7e}$$

where $\boldsymbol{T}_l^T$ is the transpose of matrix $\boldsymbol{T}_l$. Due to the appropriate choice of boundary conditions, Equations (7b) and (7c), we now may write $P[\boldsymbol{\psi}, \boldsymbol{\psi}^\dagger]$ as

$$P[\boldsymbol{\psi}, \boldsymbol{\psi}^\dagger] = -\sum_{g=1}^{G} \int_0^1 \mu \left[f_{1,g}(\mu) \psi_g^\dagger(0, \mu) + f_{2,g}(\mu) \psi_g^\dagger(Z, -\mu) \right] d\mu. \tag{8}$$

Here $f_{i,g}$, $i = 1, 2$, and $\psi_g^\dagger$ are the g-th group components of $\boldsymbol{f}_i$ and $\boldsymbol{\psi}^\dagger$, respectively.

We remark that the adjoint transport operator $\mathcal{L}^\dagger$ defined in Equation (7e) is quite similar to $\mathcal{L}$ in Equation (5e), and we refer to Prinja and Larsen (2010) for details on its derivation, with an alternative definition of the inner product, Equation (4).

Now, for a fixed particle detector, if we assume we know the adjoint flux, any given source of particles $\boldsymbol{q}$ requires only the evaluation, when possible, of Equation (6) to compute the absorption rate. Furthermore, the dependence of Equation (6) on $\boldsymbol{q}$ is linear, a fundamental feature for the source estimation problem, as discussed later in Section 5.

In the next section, we develop an analytical solution with respect to the spatial variable to the discrete ordinates model of the adjoint transport problem defined in Equation (7).

3. An ADO solution

Since the transport problem defined in Equation (7) is linear, we write its solution as a superposition of homogeneous and particular solutions to Equation (7a). Thus, we start by seeking a solution to the homogeneous equation.

3.1. Homogeneous solution

We follow our previous paper on the monoenergetic adjoint transport equation (Pazinatto et al. 2016) and the work of Siewert (2000) for the ADO solution of the multigroup transport equation, to derive an ADO solution for the adjoint to the multigroup transport equation. Thus, we start by writing the homogeneous version of Equation (7a) ($\boldsymbol{\sigma_d} = \mathbf{0}$) in the form

$$-\mu\frac{\partial}{\partial z}\boldsymbol{\psi}^{\dagger}_{\boldsymbol{h}k}(z,\mu) + \boldsymbol{S}_k\boldsymbol{\psi}^{\dagger}_{\boldsymbol{h}k}(z,\mu) = \frac{1}{2}\sum_{l=0}^{L}P_l(\mu)\boldsymbol{T}^T_{l,k}\int_0^1 P_l(\mu')\left[\boldsymbol{\psi}^{\dagger}_{\boldsymbol{h}k}(z,\mu') + (-1)^l\boldsymbol{\psi}^{\dagger}_{\boldsymbol{h}k}(z,-\mu')\right]d\mu', \tag{9}$$

where $k = 1,\ldots,R, z \in (z_{k-1}, z_k)$ and $\boldsymbol{\psi}^{\dagger}_{\boldsymbol{h}k}$ is the restriction of $\boldsymbol{\psi}^{\dagger}_{\boldsymbol{h}}$ over $[z_{k-1}, z_k]$. As we follow the same procedure within each region k and the following steps do not depend on k, we drop the subscript k in order to simplify the notation. Therefore, for an arbitrary choice of a quadrature scheme over the half-range $(0,1)$, we rewrite Equation (9) as a system of $2NG = 2 \times N \times G$ ordinary differential equations

$$-\mu_j\frac{d}{dz}\boldsymbol{\psi}^{\dagger}_{\boldsymbol{h}}(z,\mu_j) + \boldsymbol{S}\boldsymbol{\psi}^{\dagger}_{\boldsymbol{h}}(z,\mu_j) = \frac{1}{2}\sum_{l=0}^{L}P_l(\mu_j)\boldsymbol{T}^T_l\sum_{n=1}^{N}w_nP_l(\mu_n)\left[\boldsymbol{\psi}^{\dagger}_{\boldsymbol{h}}(z,\mu_n) + (-1)^l\boldsymbol{\psi}^{\dagger}_{\boldsymbol{h}}(z,-\mu_n)\right], \tag{10a}$$

and

$$\mu_j \frac{d}{dz}\boldsymbol{\psi}_{\boldsymbol{h}}^{\dagger}(z,-\mu_j) + \boldsymbol{S}\boldsymbol{\psi}_{\boldsymbol{h}}^{\dagger}(z,-\mu_j)$$
$$= \frac{1}{2}\sum_{l=0}^{L} P_l(\mu_j)\boldsymbol{T}_l^T \sum_{n=1}^{N} w_n P_l(\mu_n)\left[\boldsymbol{\psi}_{\boldsymbol{h}}^{\dagger}(z,-\mu_n) + (-1)^l \boldsymbol{\psi}_{\boldsymbol{h}}^{\dagger}(z,\mu_n)\right], \tag{10b}$$

for $j = 1, ..., N$, where μ_n and w_n are, respectively, nodes and weights of the quadrature scheme. This way, $\pm\mu_n$ are the discrete ordinates for the full-range $[-1, 1]$.

Proceeding, we seek for spectral solutions for Equations (10a) and (10b) of the form (Siewert 2000)

$$\boldsymbol{\psi}_{\boldsymbol{h}}^{\dagger}(z,\mu) = \boldsymbol{\phi}(\nu,\mu)\mathrm{e}^{-z/\nu}, \quad z \in [z_{k-1}, z_k] \tag{11}$$

for $\mu = \pm\mu_n$, where $\phi(\nu,\mu) \in \mathbb{R}^G$ and ν is a constant. If, we substitute Equation (11) into Equations (10a) and (10b), we obtain, after some algebraic manipulations, a system of $2NG$ algebraic equations

$$\left(\boldsymbol{S} + \frac{\mu_j}{\nu}\boldsymbol{I}_G\right)\phi(\nu,\mu_j) = \frac{1}{2}\sum_{l=0}^{L} P_l(\mu_j)\boldsymbol{T}_l^T \times \sum_{n=1}^{N} w_n P_l(\mu_n)\left[\boldsymbol{\phi}(\nu,\mu_n) + (-1)^l \boldsymbol{\phi}(\nu,-\mu_n)\right], \tag{12a}$$

and

$$\left(\boldsymbol{S} - \frac{\mu_j}{\nu}\boldsymbol{I}_G\right)\phi(\nu,-\mu_j) = \frac{1}{2}\sum_{l=0}^{L} P_l(\mu_j)\boldsymbol{T}_l^T \times \sum_{n=1}^{N} w_n P_l(\mu_n)\left[\boldsymbol{\phi}(\nu,-\mu_n) + (-1)^l \boldsymbol{\phi}(\nu,\mu_n)\right], \tag{12b}$$

where $j = 1, ..., N$ and $\boldsymbol{I}_G$ is the identity matrix in $\mathbb{R}^G$. Before moving further, we first need a few definitions, as described in Siewert (2000), we introduce NG-dimensional vectors ($NG = N \times G$)

$$\boldsymbol{\Phi}_+(\nu) = \left[\boldsymbol{\phi}^T(\nu,\mu_1) \ \cdots \ \boldsymbol{\phi}^T(\nu,\mu_N)\right]^T, \tag{13a}$$

and

$$\boldsymbol{\Phi}_-(\nu) = \left[\boldsymbol{\phi}^T(\nu,-\mu_1) \ \cdots \ \boldsymbol{\phi}^T(\nu,-\mu_N)\right]^T. \tag{13b}$$

In addition, we set $NG \times NG$ matrices

$$\boldsymbol{M} = \mathrm{diag}(\mu_1\boldsymbol{I}_G, ..., \mu_N\boldsymbol{I}_G), \tag{13c}$$

$$\boldsymbol{W} = \mathrm{diag}(w_1\boldsymbol{I}_G, ..., w_N\boldsymbol{I}_G), \tag{13d}$$

and

$$\boldsymbol{D} = \text{diag}\overbrace{(\boldsymbol{S}, ..., \boldsymbol{S})}^{N\text{ times}}. \tag{13e}$$

Finally, we define $NG \times G$ matrices

$$\boldsymbol{\Pi}_l = \begin{bmatrix} P_l(\mu_1)\boldsymbol{I}_G & \cdots & P_l(\mu_N)\boldsymbol{I}_G \end{bmatrix}^T, \tag{13f}$$

where $l = 1, ..., L$.

We continue to follow Siewert (2000) and we rewrite Equations (12a) and (12b) as

$$\left(\boldsymbol{D} + \frac{1}{\nu}\boldsymbol{M}\right)\boldsymbol{\Phi}_+(\nu) = \frac{1}{2}\sum_{l=0}^{L}\boldsymbol{\Pi}_l\boldsymbol{T}_l^T\boldsymbol{\Pi}_l^{\mathrm{T}}\boldsymbol{W}\Big[\boldsymbol{\Phi}_+(\nu) + (-1)^l\boldsymbol{\Phi}_-(\nu)\Big], \tag{14a}$$

and

$$\left(\boldsymbol{D} - \frac{1}{\nu}\boldsymbol{M}\right)\boldsymbol{\Phi}_-(\nu) = \frac{1}{2}\sum_{l=0}^{L}\boldsymbol{\Pi}_l\boldsymbol{T}_l^T\boldsymbol{\Pi}_l^{\mathrm{T}}\boldsymbol{W}\Big[\boldsymbol{\Phi}_-(\nu) + (-1)^l\boldsymbol{\Phi}_+(\nu)\Big]. \tag{14b}$$

Aiming to explore the symmetry found in Equations (14a) and (14b), we also define NG-dimensional vectors

$$\boldsymbol{U}(\nu) = \boldsymbol{\Phi}_+(\nu) + \boldsymbol{\Phi}_-(\nu), \tag{15a}$$

and

$$\boldsymbol{V}(\nu) = \boldsymbol{\Phi}_+(\nu) - \boldsymbol{\Phi}_-(\nu). \tag{15b}$$

Then, we add Equations (14a) and (14b) to obtain

$$\boldsymbol{D} - \frac{1}{2}\sum_{l=0}^{L}\boldsymbol{\Pi}_l\boldsymbol{T}_l^T\boldsymbol{\Pi}_l^{\mathrm{T}}\boldsymbol{W}\Big[1 + (-1)^l\Big]\Big)\boldsymbol{U}(\nu) = -\frac{1}{\nu}\boldsymbol{M}\boldsymbol{V}(\nu), \tag{16a}$$

and, similarly, we subtract Equation (14b) from Equation (14a), to obtain

$$\boldsymbol{D} - \frac{1}{2}\sum_{l=0}^{L}\boldsymbol{\Pi}_l\boldsymbol{T}_l^T\boldsymbol{\Pi}_l^{\mathrm{T}}\boldsymbol{W}\Big[1 - (-1)^l\Big]\Big)\boldsymbol{V}(\nu) = -\frac{1}{\nu}\boldsymbol{M}\boldsymbol{U}(\nu). \tag{16b}$$

We now introduce the $NG \times NG$ matrices

$$\boldsymbol{A} = \quad \boldsymbol{D} - \frac{1}{2}\sum_{l=0}^{L}\boldsymbol{\Pi}_l\boldsymbol{T}_l^T\boldsymbol{\Pi}_l^{\mathrm{T}}\boldsymbol{W}\Big[1 + (-1)^l\Big]\Big)\boldsymbol{M}^{-1}, \tag{17a}$$

and

$$\boldsymbol{B} = \quad \boldsymbol{D} - \frac{1}{2}\sum_{l=0}^{L}\boldsymbol{\Pi}_l\boldsymbol{T}_l^T\boldsymbol{\Pi}_l^{\mathrm{T}}\boldsymbol{W}\Big[1 - (-1)^l\Big]\Big)\boldsymbol{M}^{-1}, \tag{17b}$$

and NG-dimensional vectors

$$\boldsymbol{X}(\nu) = \boldsymbol{M}\boldsymbol{U}(\nu), \tag{17c}$$

and

$$\boldsymbol{Y}(\nu) = \boldsymbol{M}\boldsymbol{V}(\nu), \tag{17d}$$

to rewrite both equations in (16) as

$$\boldsymbol{A}\boldsymbol{X}(\nu) = -\frac{1}{\nu}\boldsymbol{Y}(\nu) \tag{18a}$$

and

$$\boldsymbol{B}\boldsymbol{Y}(\nu) = -\frac{1}{\nu}\boldsymbol{X}(\nu), \tag{18b}$$

respectively. This way, we use Equation (18b) to remove $\boldsymbol{Y}(\nu)$ from Equation (18a), which leads us to the following NG-dimensional eigenvalue problem

$$\boldsymbol{B}\boldsymbol{A}\boldsymbol{X}(\nu) = \frac{1}{\nu^2}\boldsymbol{X}(\nu). \tag{19a}$$

Alternatively, we could have used Equation (18a) to get rid of $\boldsymbol{X}(\nu)$ in Equation (18b) in order to get the following NG-dimensional eigenvalue problem

$$\boldsymbol{A}\boldsymbol{B}\boldsymbol{Y}(\nu) = \frac{1}{\nu^2}\boldsymbol{Y}(\nu). \tag{19b}$$

We might use either Equation (19a) or Equation (19b) to obtain constants ν and subsequently eigenfunctions $\boldsymbol{\phi}(\nu, \mu)$ for Equation (11). Therefore, we multiply Equation (18a) by $-\nu$, add $\boldsymbol{X}(\nu)$ on the resulting equation and use definitions Equations (15) and (17) to get

$$\boldsymbol{\Phi}_{+}(\nu) = \frac{1}{2}\boldsymbol{M}^{-1}(\boldsymbol{I}_{NG} - \nu\boldsymbol{A})\boldsymbol{X}(\nu), \tag{20a}$$

where $\boldsymbol{I}_{NG}$ is the $NG \times NG$ identity matrix. In a similar way, we multiply Equation (18a) by ν and add $\boldsymbol{X}(\nu)$ to get the result

$$\boldsymbol{\Phi}_{-}(\nu) = \frac{1}{2}\boldsymbol{M}^{-1}(\boldsymbol{I}_{NG} + \nu\boldsymbol{A})\boldsymbol{X}(\nu). \tag{20b}$$

From Equations (19a) (or (19b)), (20a) and (20b), we can easily show that

$$\boldsymbol{\Phi}_{+}(-\nu) = \frac{1}{2}\boldsymbol{M}^{-1}(\boldsymbol{I}_{NG} + \nu\boldsymbol{A})\boldsymbol{X}(\nu) = \boldsymbol{\Phi}_{-}(\nu), \tag{21a}$$

and

$$\boldsymbol{\Phi}_{-}(-\nu) = \frac{1}{2}\boldsymbol{M}^{-1}(\boldsymbol{I}_{NG} - \nu\boldsymbol{A})\boldsymbol{X}(\nu) = \boldsymbol{\Phi}_{+}(\nu), \tag{21b}$$

We use that to write the homogeneous solution to the discrete ordinates model of the adjoint equation to the multigroup transport equation. We still note that due the similarity between the transport Equation (5a) and its adjoint (7a), the eigenvalue problems defined by Equations (19a) and (19b) are exactly the same as the ones found by Siewert (2000). However, the eigenfunctions in Equations (20a) and (20b) appear with the ± signs, before ν, interchanged with respect to the ADO eigenfunctions of the forward problem. Then, we can easily change our existing ADO code for the forward transport problem to handle the adjoint transport problem.

At this point, we bring back the k subscript and assume that we obtain a complete set of $2NGR$ numbers $\pm\nu_{i,k}, i = 1, \ldots, NG$, and eigenfunction $\boldsymbol{\Phi}_{+,k}$ and $\boldsymbol{\Phi}_{-,k}$, for each region k, $k = 1, \ldots, R$. Thus, for a fixed region k, we define NG-dimensional vectors

$$\boldsymbol{\Psi}^{\dagger}_{\boldsymbol{h}+,k}(z) = \left[\boldsymbol{\psi}^{\dagger}_{\boldsymbol{h}k}{}^{\mathrm{T}}(z,\mu_1) \quad \cdots \quad \boldsymbol{\psi}^{\dagger}_{\boldsymbol{h}k}{}^{\mathrm{T}}(z,\mu_{\mathrm{N}})\right]^{\mathrm{T}}, \tag{22a}$$

and

$$\boldsymbol{\Psi}^{\dagger}_{\boldsymbol{h}-,k}(z) = \left[\boldsymbol{\psi}^{\dagger}_{\boldsymbol{h}k}{}^{\mathrm{T}}(z,-\mu_1) \quad \cdots \quad \boldsymbol{\psi}^{\dagger}_{\boldsymbol{h}k}{}^{\mathrm{T}}(z,-\mu_{\mathrm{N}})\right]^{\mathrm{T}}, \tag{22b}$$

and write a homogeneous solution of the adjoint discrete ordinates equations as a linear combination of the proposed solutions (11) for each $\pm\nu_{i,k}$. Therefore, we write

$$\boldsymbol{\Psi}^{\dagger}_{\boldsymbol{h}+,k}(z) = \sum_{\mathrm{i}=1}^{\mathrm{NG}}\left[\mathrm{A}_{\mathrm{i},k}\boldsymbol{\Phi}_{+,k}(\nu_{\mathrm{i},k})\mathrm{e}^{-(z-z_{k-1})/\nu_{\mathrm{i},k}} + \mathrm{B}_{\mathrm{i},k}\boldsymbol{\Phi}_{-,k}(\nu_{\mathrm{i},k})\mathrm{e}^{-(z_k-z)/\nu_{\mathrm{i},k}}\right], \tag{23a}$$

and

$$\boldsymbol{\Psi}^{\dagger}_{\boldsymbol{h}-,k}(z) = \sum_{\mathrm{i}=1}^{\mathrm{NG}}\left[\mathrm{A}_{\mathrm{i},k}\boldsymbol{\Phi}_{-,k}(\nu_{\mathrm{i},k})\mathrm{e}^{-(z-z_{k-1})/\nu_{\mathrm{i},k}} + \mathrm{B}_{\mathrm{i},k}\boldsymbol{\Phi}_{+,k}(\nu_{\mathrm{i},k})\mathrm{e}^{-(z_k-z)/\nu_{\mathrm{i},k}}\right], \tag{23b}$$

for $k = 1, \ldots, R$ and $z \in [z_{k-1}, z_k]$, with shifted exponentials in order to avoid numerical overflow.

To determine $2NGR$ constants $A_{i,k}$ and $B_{i,k}, i = 1, \ldots, NG$ and $k = 1, \ldots, R$, we must present a particular solution to Equation (7a), as we do next.

3.2. General solution

Given the linearity of Equation (7a), we can write its general solution as a sum of the already established homogeneous solution plus a particular solution. In this work, we consider only particle detectors with constant

absorption within a fixed region k, $k = 1, \ldots, R$. Therefore, we may seek a G-dimensional constant vector $\boldsymbol{\psi}^{\dagger}_{\boldsymbol{p}k}$ as a particular solution of Equation (7a). We substitute $\boldsymbol{\psi}^{\dagger}_{\boldsymbol{p}k}$ into (7a) and we assume $\boldsymbol{\sigma}_{\boldsymbol{d}k}$, the restriction of $\boldsymbol{\sigma}_{\boldsymbol{d}}$ to $[z_{k-1}, z_k]$, as given in Equation (2), such that

$$\boldsymbol{S}_{\boldsymbol{k}}\boldsymbol{\psi}^{\dagger}_{\boldsymbol{p}k} = \boldsymbol{T}^{\mathrm{T}}_{0,k}\boldsymbol{\psi}^{\dagger}_{\boldsymbol{p}k} + \boldsymbol{\sigma}_{\boldsymbol{d}k}. \tag{24}$$

After some algebraic manipulation, we obtain

$$\boldsymbol{\psi}^{\dagger}_{\boldsymbol{p}k} = \left(\boldsymbol{S}_{\boldsymbol{k}} - \boldsymbol{T}^{\mathrm{T}}_{0,k}\right)^{-1}\boldsymbol{\sigma}_{\boldsymbol{d}k}, \quad z \in [z_{k-1}, z_k], \tag{25}$$

for $k = 1, \ldots, R$, provided that $\boldsymbol{S}_{\boldsymbol{k}} - \boldsymbol{T}^{T}_{0,k}$ is a nonsingular matrix.

To conclude the ADO formulation, we define NG-dimensional vectors

$$\boldsymbol{\Psi}^{\dagger}{}_{+,k}(z) = \left[\boldsymbol{\psi}^{\dagger T}_{k}(z, \mu_1) \quad \cdots \quad \boldsymbol{\psi}^{\dagger T}_{k}(z, \mu_N)\right]^{T}, \tag{26a}$$

and

$$\boldsymbol{\Psi}^{\dagger}{}_{-,k}(z) = \left[\boldsymbol{\psi}^{\dagger T}_{k}(z, -\mu_1) \quad \cdots \quad \boldsymbol{\psi}^{\dagger T}_{k}(z, -\mu_N)\right]^{T}, \tag{26b}$$

in order to write a general solution for discrete ordinates model of the adjoint equation as

$$\boldsymbol{\Psi}^{\dagger}{}_{+,k}(z) = \sum_{i=1}^{NG}\left[A_{i,k}\boldsymbol{\Phi}_{+,k}(\nu_{i,k})e^{-(z-z_{k-1})/\nu_{i,k}} + B_{i,k}\boldsymbol{\Phi}_{-,k}(\nu_{i,k})e^{-(z_k-z)/\nu_{i,k}}\right] + \boldsymbol{\Psi}^{\dagger}_{\boldsymbol{p}k}, \tag{27a}$$

and

$$\boldsymbol{\Psi}^{\dagger}{}_{-,k}(z) = \sum_{i=1}^{NG}\left[A_{i,k}\boldsymbol{\Phi}_{-,k}(\nu_{i,k})e^{-(z-z_{k-1})/\nu_{i,k}} + B_{i,k}\boldsymbol{\Phi}_{+,k}(\nu_{i,k})e^{-(z_k-z)/\nu_{i,k}}\right] + \boldsymbol{\Psi}^{\dagger}_{\boldsymbol{p}k}, \tag{27b}$$

for $k = 1, \ldots, R, z \in [z_{k-1}, z_k]$ and the particular component $\boldsymbol{\Psi}^{\dagger}_{\boldsymbol{p}k}$ defined as

$$\boldsymbol{\Psi}^{\dagger}_{\boldsymbol{p}_k} = \overbrace{\left[\boldsymbol{\psi}^{\dagger^{\mathrm{T}}}_{\mathrm{p}_k} \ldots \boldsymbol{\psi}^{\dagger^{\mathrm{T}}}_{\mathrm{p}_k}\right]}^{\text{N times}}. \tag{28}$$

To establish the general solution we have to determine the unknown constants $A_{i,j}$ and $B_{i,j}$. To do that we generate and solve a $2NGR$ order linear system from the boundary conditions, Equations (7b) and (7c), and the continuity requirements stated in Equation (7d).

Once we have the ADO solution to the adjoint transport Equation (7a), we may explore its analyticity with respect to the spatial variable to derive explicit expressions for the absorption rate of particles of an internal detector.

Before proceeding, we note that Siewert (2000) derived a particular solution for the multigroup forward transport problem that is useful for more general source terms. Such formulation may be extended to deal also with adjoint problems with source terms defined by more general functions.

3.3. Explicit formulas for the absorption rate

Since we consider a multilayer slab composed of R contiguous regions, as indicated in Equation (1), we can rewrite the integral term in the absorption rate definition, Equation (6), as

$$r = \langle \boldsymbol{\psi}^{\dagger}, \boldsymbol{q} \rangle - P[\boldsymbol{\psi}, \boldsymbol{\psi}^{\dagger}] = \sum_{g=1}^{G} \sum_{k=1}^{R} \int_{z_{k-1}}^{z_k} \int_{-1}^{1} \psi_{g,k}^{\dagger}(z,\mu) q_{g,k}(z,\mu) d\mu dz - P\left[\boldsymbol{\psi}, \boldsymbol{\psi}^{\dagger}\right], \tag{29}$$

where for each region k, $q_{g,k}(z,\mu)$ are the components, for each energy group g, $g = 1, \ldots, G$, of the internal source vector $\boldsymbol{q}_k, k = 1, \ldots, R$. If we assume $\boldsymbol{q}_k$ is piecewise constant over the slab regions and $\boldsymbol{f}_1$ and $\boldsymbol{f}_2$ are constant vectors (representing the incoming fluxes at the boundaries, such that, $f_{1,g}$ and $f_{2,g}$ are also constants for each energy group g), Equation (29) takes the form

$$r = \sum_{g=1}^{G} \left[\sum_{k=1}^{R} \left(\phi_{g,k} + 2(z_k - z_{k-1}) \psi_{p,g,k}^{\dagger} \right) q_{g,k} + \hat{\phi}_g + \frac{f_{1,g}}{2} \psi_{p,g,1}^{\dagger} + \frac{f_{2,g}}{2} \psi_{p,g,R}^{\dagger} \right], \tag{30a}$$

where the terms inside the first parenthesis, in Equation (30a), represent the contribution of the inner product defined in Equation (4) to the absorption rate. We note that in deriving Equation (29) we used the fact that the particular solution is given as in Equation (25), and we define

$$\phi_{g,k} = \sum_{i=1}^{NG} \nu_{i,k} (A_{i,k} + B_{i,k}) \left(1 - e^{-(z_k - z_{k-1})/\nu_{i,k}}\right) \phi_{i,g,k}, \tag{30b}$$

and

$$\phi_{i,g,k} = \sum_{n=1}^{N} w_n \left[\phi_g(\nu_{i,k}, \mu_n) + \phi_g(\nu_{i,k}, -\mu_n) \right]. \tag{30c}$$

The remaining terms in Equation (30a) add the contribution of the boundary term (8) to the absorption rate, where

$$\hat{\phi}_g = \sum_{i=1}^{NG} \sum_{n=1}^{N} w_n \mu_n \left[\hat{\phi}_{g,i,n,1} f_{1,g} + \hat{\phi}_{g,i,n,R} f_{2,g} \right], \tag{30d}$$

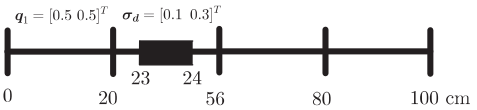

Figure 2. Test problem.

with

$$\hat{\phi}_{g,i,n,1} = A_{i,1}\phi_g(\nu_{i,1}, \mu_n) + B_{i,1}\phi_g(\nu_{i,1}, -\mu_n)e^{-z_1/\nu_{i,1}}, \tag{30e}$$

and

$$\hat{\phi}_{g,i,n,R} = A_{i,R}\phi_g(\nu_{i,R}, -\mu_n)e^{-(Z-z_{R-1})/\nu_{i,R}} + B_{i,R}\phi_g(\nu_{i,R}, +\mu_n). \tag{30f}$$

For a more general approach, if $\boldsymbol{q}$ depends either on the spatial variable z or on the direction μ, it may be necessary to work on the evaluation of integrals like

$$\int_a^b q_{g,k}(z,\mu)e^{-(z-\alpha)/\nu}dz, \quad \int_a^b q_{g,k}(z,\mu)e^{-(\beta-z)/\nu}dz, \tag{31}$$

with $[a,b] \subseteq [\alpha,\beta]$, for $k = 1, ..., R$ and $g = 1, ..., G$. However, as we will see later on in this text, when discussing source estimation, those general integral evaluations may be avoided when the source is expanded in a convenient (piecewise constant) basis. Still, when dealing with the dependency of $\boldsymbol{f}_1$ and $\boldsymbol{f}_2$ on μ, special attention has to be given to the integrals defined in Equation (8).

In the next section, we test the proposed method for solving the adjoint transport equation. We compute absorption rates using Equation (6) and we compare them with results obtained from Equation (3).

4. Source-detector test problem

In order to test the derived ADO solution for adjoint transport problems, we estimate the absorption rate using Equation (6), and then we compare with results obtained from Equation (3), by implementing the ADO method (Siewert 2000) for solving the forward problem, Equation (5a). Thus, we consider a two-groups problem in a four-layer slab defined for $z \in [0, 100]$, according to Figure 2, as stated by Barros and Larsen (1991), with reflecting boundary condition at $z = 0$ and vacuum at $z = 100$,

$$\boldsymbol{\psi}(0,\mu) = \boldsymbol{\psi}(0,-\mu), \tag{32a}$$

$$\boldsymbol{\psi}(100,-\mu) = \boldsymbol{0}, \tag{32b}$$

for $\mu \in (0, 1]$.

Continuing, there is an internal source of particles $\boldsymbol{q}$ defined within the slab, with $\boldsymbol{q}_k = \boldsymbol{0}$ for region k, k = 2, 3, 4. For the first region, k = 1, we set $\boldsymbol{q}_1$ as

Table 1. Absorption rates of particles migrating from all directions and energy groups within the range [23,24].

N	r	$r^{\dagger}$
2	0.19672070465	0.19672070465
4	0.19618914572	0.19618914572
8	0.19618610963	0.19618610963
16	0.19618610990	0.19618610990
32	0.19618610982	0.19618610982
64	0.19618610981	0.19618610981

The estimated value computed using Equation (3) is represented by r, and the value estimated by Equation (6) is $r^{\dagger}$.

$$\boldsymbol{q}_1(z,\mu) = \begin{pmatrix} 0.5 \\ 0.5 \end{pmatrix}, \tag{33}$$

for $z \in [0, 20]$ and $\mu \in [-1, 1]$. In addition, total macroscopic cross sections (cm^{-1}) and group transfer cross sections (cm^{-1}) are, for each region k, $k = 1, 2, 3, 4$, given by Barros and Larsen (1991)

$$\boldsymbol{S}_1 = \begin{bmatrix} 1.00 & 0.00 \\ 0.00 & 1.20 \end{bmatrix}, \quad \boldsymbol{T}_{0,1} = \begin{bmatrix} 0.90 & 0.05 \\ 0.20 & 0.80 \end{bmatrix}, \tag{34a}$$

$$\boldsymbol{S}_2 = \begin{bmatrix} 0.90 & 0.00 \\ 0.00 & 1.50 \end{bmatrix}, \quad \boldsymbol{T}_{0,2} = \begin{bmatrix} 0.75 & 0.10 \\ 0.30 & 0.99 \end{bmatrix}, \tag{34b}$$

$$\boldsymbol{S}_3 = \begin{bmatrix} 1.10 & 0.00 \\ 0.00 & 0.85 \end{bmatrix}, \quad \boldsymbol{T}_{0,3} = \begin{bmatrix} 0.95 & 0.00 \\ 0.60 & 0.20 \end{bmatrix}, \tag{34c}$$

and

$$\boldsymbol{S}_4 = \begin{bmatrix} 1.00 & 0.00 \\ 0.00 & 1.20 \end{bmatrix}, \quad \boldsymbol{T}_{0,4} = \begin{bmatrix} 0.90 & 0.05 \\ 0.20 & 0.80 \end{bmatrix}, \tag{34d}$$

respectively. To complete the problem, in the interior of the slab, there is a particle detector, to which we define the absorption cross section $\boldsymbol{\sigma_d}$ as

$$\boldsymbol{\sigma}_d(z,\mu) = \begin{cases} \begin{pmatrix} 0.1 \\ 0.3 \end{pmatrix}, & z \in [23, 24], \\ \boldsymbol{0}, & \text{otherwise.} \end{cases} \tag{35}$$

We note that, with respect to the choice of a quadrature scheme for defining the discrete ordinates, we follow our previous works and choose to generate a standard Gauss-Legendre quadrature (Golub and Welsch 1969), and then map the nodes and weights from the full-range $[-1, 1]$ to the half-range $[0, 1]$ interval.

Before comparing our results for absorption rates computed from both ADO solutions, the adjoint and forward equations, we checked our scalar fluxes data with the ones listed by Barros and Larsen (1991), but we did not find agreement. In fact, according to one of the authors (R.C. Barros,

personal communication, 2017), the results listed in Barros and Larsen (1991) were later corrected by an alternative implementation using the Response Matrix method (R. Barros and O. Silva, private communication, 2017). In this way, we then found agreement, in eight to ten digits, between our results obtained either via the ADO method or our implementation of the *Diamond Difference* method (Lewis and Miller 1984) and R. Barros and O. Silva (private communication, 2017) results.

In Table 1 we display numerical results for the absorption rate r estimated from Equation (3), $r^\dagger$ from Equation (6), using $N = 2, 4, 8, 16, 32, 64$. We applied the explicit formula, Equation (30a), for the absorption rate to generate this table. As we can see, all results were the same using the transport problem (5) and the adjoint problem (7) for all tested values of N, with the number of displayed figures limited by angular convergence. In fact, $|r - r^\dagger| = O(10^{-16})$ for every N tested. However, the same performance was not obtained when using numerical integration in the spatial variable, when evaluating Equation (6). In such case, our best result was $|r - r^\dagger| = O(10^{-10})$. Besides of that, the test using analytical formulas took less than a second to be executed in our computer (equipped with an Intel Core i5-4670 processor), around a hundred times faster than when we used numerical integration in the z variable.

In the next section, we introduce an inverse problem of source estimation to further test the ADO adjoint formulation.

5. Source estimation

According to Beck and Arnold (1977), parameter estimation can be seen as a study of inverse problems. When not all parameters in a mathematical model are known but discrete measurements related to the dependent variable inside the domain are given instead, these can be used to estimate values for the unknowns. Here we consider an isotropic source $\boldsymbol{q}$ within a physical domain, a slab, to which all physical properties are known as well as incoming fluxes at the boundaries. We assume that we are able to approximate this source on a given linear space once we estimate the coefficients of a basis expansion. This way, we aim to estimate $\boldsymbol{q}$ using known information that might be inaccurate due measurement errors, of the absorption rate from a set of internal particle detectors.

To reach this goal, our first step is to find a model that relates the absorption rate of particles with the coefficients of an approximation of the source in a given basis. We then suppose that

i. a set of D particle detectors is placed within the slab $(0, Z)$, each one of them providing a reading, called $r_{i,g}$, for each energy group (Hykes and Azmy 2011);

ii. $\boldsymbol{\sigma}_{\boldsymbol{d}i,g}$ is the absorption cross section related to the g-th energy group of the i-th detector. Thus, from (i) and Equation (2), the only non-zero component of $\boldsymbol{\sigma}_{\boldsymbol{d}i,g}$ is the g-th component of the vector;
iii. for each detector, the adjoint angular flux that solves Equation (7a), with $\boldsymbol{\sigma}_{\boldsymbol{d}i,g}$ in the right hand side, is available;
iv. we may approximate $\boldsymbol{q}$ by $\tilde{\boldsymbol{q}} = [\tilde{q}_1 \cdots \tilde{q}_G]^T$, with

$$\tilde{q}_g(z) = \sum_{b=1}^{B_g} \alpha_{b,g} \tilde{q}_{b,g}(z), \tag{36}$$

for $g = 1, ..., G$. Here $\tilde{q}_{b,g}, b = 1, ..., B_g$, correspond to a set of basis functions defined for $z \in [0, Z]$, and $\alpha_{b,g}$ are the targets of our estimation process.

Thus, we introduce DG-dimensional vectors

$$\boldsymbol{r} = \left[\overbrace{r_{1,1} \ldots r_{1,G}}^{\text{detector 1}} \ldots \overbrace{r_{D,1} \ldots r_{D,G}}^{\text{detector D}}\right]^T, \tag{37a}$$

and, using Equation (8),

$$\boldsymbol{p}_g = \left[\overbrace{p_{1,g} \cdots p_{D,g}}^{\text{group g}}\right]^T. \tag{37b}$$

for $g = 1, ..., G$, with

$$p_{i,g} = -\int_0^1 \mu \left[\psi^\dagger_{i,g}(0, \mu) f_{1,g}(\mu) + \psi^\dagger_{i,g}(Z, -\mu) f_{2,g}(\mu)\right] d\mu, \tag{37c}$$

for $i = 1, ..., D$. In addition, we define $DG \times B_g$ matrices $\boldsymbol{A}_g = [A_{i,b,g}]$, whose components we write as

$$A_g = \int_{-1}^1 \int_0^Z \psi^\dagger_{i,g}(z, \mu) \tilde{q}_{b,g} dz d\mu, \tag{37d}$$

in order to rewrite $\boldsymbol{r}$ in Equation (37a) as

$$\boldsymbol{r}(\boldsymbol{\alpha}_1, ..., \boldsymbol{\alpha}_G) = \sum_{g=1}^{G} [\boldsymbol{A}_g \boldsymbol{\alpha}_g - \boldsymbol{p}_g]. \tag{38}$$

Before proceeding, we must choose a set of basis functions to approximate each component $\boldsymbol{q}_g$ of $\boldsymbol{q}$. In this work, we equally divide the range $[0, Z]$ in contiguous intervals and consider, as basis functions, the characteristic function of each interval. This way, we define for $B \in \mathbb{N}$, basis functions

$$\tilde{q}_{b,g} = \begin{cases} 1, & z \in \left[(b-1)h_z, bh_z\right], \\ 0, & \text{otherwise}, \end{cases} \tag{39}$$

with $h_z = Z/B, b = 1, ..., B$ and $g = 1, ..., G$, to complete our model.

We remark that, given the choice of basis function, as previous done in Section 3, we can use Equation (30a) to write explicit formulas to Equations (37c) and (37d), improving speed and accuracy. However, a different set of basis functions requires new explicit formulas to be derived.

We suppose that Equation (38) and, of course, our solution to Equation (7a) are accurate, so all error comes from the measurement process. Thus, if the DG-dimensional ($DG = D \times G$) vector $\tilde{\boldsymbol{r}}$ represents the physical measurements, we assume that

$$\tilde{\boldsymbol{r}} = \boldsymbol{r}(\boldsymbol{\alpha}_1, ..., \boldsymbol{\alpha}_G) + \boldsymbol{\epsilon} \tag{40}$$

where $\boldsymbol{\epsilon}$ is a random vector, normally distributed, with zero mean, $\boldsymbol{W}$ covariance matrix of dimension $DG \times DG$, and independent of $\boldsymbol{\alpha}_1, ..., \boldsymbol{\alpha}_G$. For short, we denote $\boldsymbol{\epsilon} \sim \mathcal{N}(\boldsymbol{0}, \boldsymbol{W})$. This way, we may write the probability density function for the error distribution as (Kaipio and Somersalo 2005)

$$\pi(\boldsymbol{\epsilon}) = (2\pi)^{-DG/2} |\boldsymbol{W}|^{-1/2} \exp\left\{ -\frac{1}{2} [\tilde{\boldsymbol{r}} - \boldsymbol{r}]^T \boldsymbol{W}^{-1} [\tilde{\boldsymbol{r}} - \boldsymbol{r}] \right\}. \tag{41}$$

Since $\pi(\boldsymbol{\epsilon})$ is centered at zero, we can estimate $\boldsymbol{\alpha_1}, ..., \boldsymbol{\alpha}_G$ by searching for the maximum value of Equation (41), which is equivalent to searching for the minimum value of its argument

$$S(\boldsymbol{\alpha}_1, ..., \boldsymbol{\alpha}_G) = \left[\tilde{\boldsymbol{r}} - \boldsymbol{r}(\boldsymbol{\alpha}_1, ..., \boldsymbol{\alpha}_G) \right]^T \boldsymbol{W}^{-1} [\tilde{\boldsymbol{r}} - \boldsymbol{r}(\boldsymbol{\alpha}_1, ..., \boldsymbol{\alpha}_G)], \tag{42}$$

which we can rewrite, using the linearity of Equation (38), as

$$S(\boldsymbol{\alpha}) = ||\boldsymbol{W}^{-1/2} [\hat{\boldsymbol{r}} - \boldsymbol{A}\boldsymbol{\alpha}]||^2, \tag{43}$$

where we defined the DG-dimensional vector

$$\hat{\boldsymbol{r}} = \tilde{\boldsymbol{r}} - \sum_{g=1}^{G} \boldsymbol{p}_g, \tag{44}$$

the BG-dimensional vector ($BG = B \times G$)

$$\boldsymbol{\alpha} = \left[\boldsymbol{\alpha}_1^{\mathrm{T}} \cdots \boldsymbol{\alpha}_G^{\mathrm{T}} \right]^{\mathrm{T}}, \tag{45}$$

and the $DG \times BG$ matrix

$$\boldsymbol{A} = [\boldsymbol{A}_1 \cdots \boldsymbol{A}_G]. \tag{46}$$

Unfortunately, we found that the minimum value of Equation (43) seems to be quite sensitive to noisy information. Thus, we apply a known regularization technique, the Tikhonov regularization, which is essentially a penalized version of Equation (43) (Kaipio and Somersalo 2005)

$$S_\lambda(\boldsymbol{\alpha}) = ||\boldsymbol{W}^{-1/2} [\hat{\boldsymbol{r}} - \boldsymbol{A}\boldsymbol{\alpha}]||^2 + \lambda^2 ||\boldsymbol{\alpha}||^2, \tag{47}$$

to search for minimal norm-2 solutions.

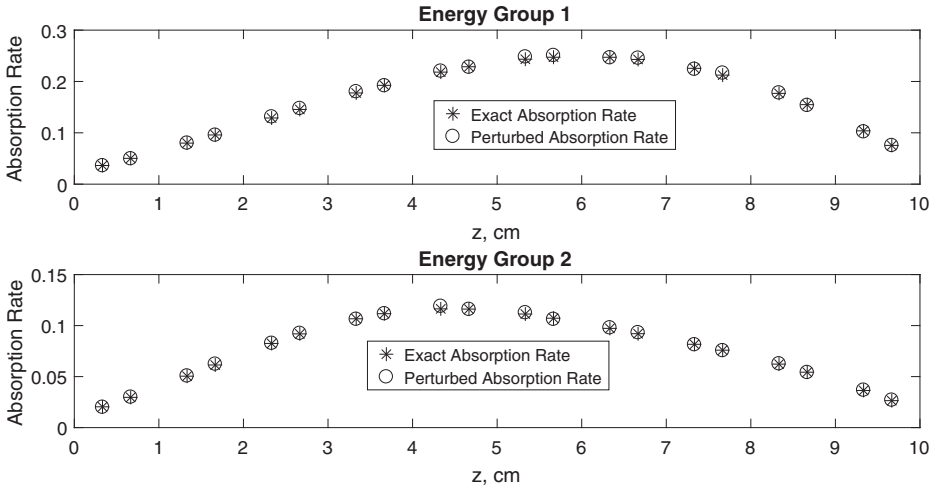

Figure 3. Absorption rates for each energy group. Asterisks represent exact data and circles indicate noisy measurements computed using W_1 as covariance matrix in Equation (40).

5.1. Test problem I

As a first test to our formulation, we consider a two-group transport problem defined in a slab, $z \in [0, 10]$, with physical properties given by Equation (34a) and vacuum boundary conditions,

$$\boldsymbol{\psi}(0, \mu) = \mathbf{0}, \tag{48a}$$

and

$$\boldsymbol{\psi}(10, -\mu) = \mathbf{0}, \tag{48b}$$

for $\mu \in [0, 1]$. We aim to estimate an internal source of particles $\boldsymbol{q} = [q_1 \; q_2]^T$, whose components are

$$q_1(z) = \frac{500}{75031} z^2(z^2 - 14z + 49), \tag{49a}$$

and

$$q_2(z) = -\frac{20}{4000} z^2(z - 10), \tag{49b}$$

for $z \in [0, 10]$.

We choose an alternate method (than ADO) to simulate measurements. In this case, we generate a vector $\boldsymbol{r_0}$, which we take as exact measurements, using our implementation of the *Diamond Difference* method (Lewis and Miller 1984), considering 128 discrete directions, 100 nodes per *cm* and a tolerance of 10^{-12}, in the iterative steps. The idea is to avoid the referred "inverse crime" (Kaipio and Somersalo 2005). In which case, the numerically given simulated data are produced by the same model that is used to invert the data and the discretization in the numerical simulation is the

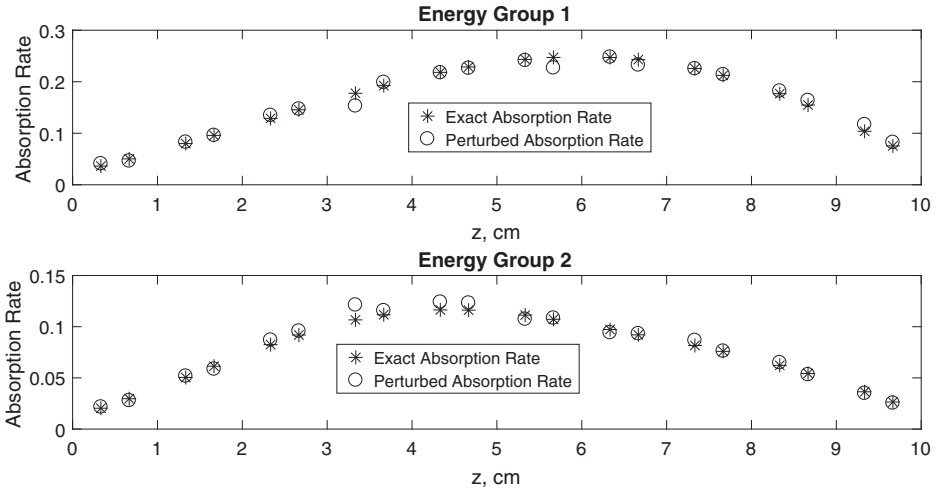

Figure 4. Absorption rates for each energy group. Asterisks represent exact data and circles indicate noisy measurements computed using $\boldsymbol{W}_2$ as covariance matrix in Equation (40).

same as the one used in the inversion. Such thing may lead to unreliable conclusions if compared to data provided by more practical situations.

Proceeding, we introduce covariance matrices $\boldsymbol{W}_1$ and $\boldsymbol{W}_2$, such that $\boldsymbol{W}_1^{1/2} = \text{diag}(0.01 \times \boldsymbol{r_0})$ and $\boldsymbol{W}_2^{1/2} = \text{diag}(0.05 \times \boldsymbol{r_0})$, in order to generate $\boldsymbol{\epsilon}_1 \sim \mathcal{N}(\boldsymbol{0}, \boldsymbol{W}_1)$ and $\boldsymbol{\epsilon}_2 \sim \mathcal{N}(\boldsymbol{0}, \boldsymbol{W}_2)$, and define perturbed data $\tilde{\boldsymbol{r}}_1$ and $\tilde{\boldsymbol{r}}_2$ using Equation (40).

Moving on, $\boldsymbol{A}$ in Equation (37d) is calculated using the adjoint ADO formulation, with $N = 4$, which is equivalent to eight discrete ordinates. We chose such a low value of N because we did not notice any difference in our source estimation results using a higher number of directions and, also, to keep the method fast. The regularization parameter λ was manually set, instead of using possible automatic approaches available in the literature (Kaipio and Somersalo 2005). In Figures 3 and 4, we display, for each energy group, the exact absorption rate and the perturbed measurements which we considered to estimate $\boldsymbol{q}$. Asterisks represent the exact data and circles indicate noisy measurements.

We note that in our tests we used only a single realization of each random vector. Thus, when comparing exact data with $\tilde{\boldsymbol{r}}_1$, we have 1.2115% of relative error, in the vector 2-norm, as we see in Figure 3. For $\tilde{\boldsymbol{r}}_2$, as we show in Figure 4, we have 5.1421% of relative error.

Proceeding, we set $B = 10$ in Equation (39) in order to define a set of basis functions for each energy group. We remark that the space generated by the basis functions defined in Equation (39) is too poor to represent $\boldsymbol{q}$, thus, we expect additional error in our source estimation. We use the L^2 norm to compute absolute and relative errors between the estimated source and the projection of the exact source into the space generated by the basis

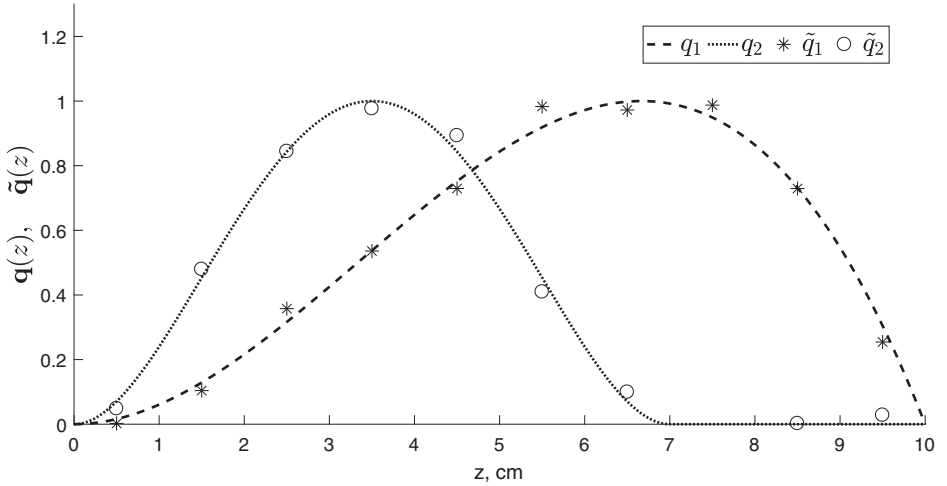

Figure 5. Components of exact and estimated sources using $\boldsymbol{W}_1$ to generate noisy measurements with Equation (40) and $B = 10$ in Equation (39). Lines represent exact component and asterisks estimated components.

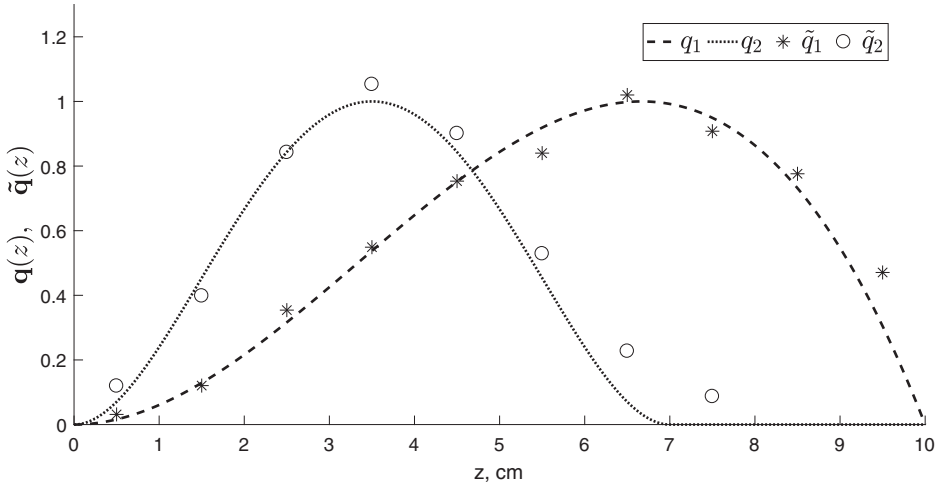

Figure 6. Components of exact and estimated sources using $\boldsymbol{W}_2$ to generate noisy measurements with Equation (40) and $B = 10$ in Equation (39). Lines represent exact component and asterisks estimated components.

functions. We consider the existence of two readings by energy group in each basis function's support. In Figures 5 and 6, we present the estimated source for each error level, using $\boldsymbol{W}_1$ and $\boldsymbol{W}_2$, respectively. Lines are used to represent each component of $\boldsymbol{q}$, and asterisks to each estimated component of $\tilde{\boldsymbol{q}}$.

As we can see in Figure 5, using $\boldsymbol{W}_1$ to generate noisy readings, the estimation process was able to recover the shape of the exact source and its magnitude. Moreover, when we compute the error, the first energy group displayed an absolute error of 0.1090, which implied a relative error of

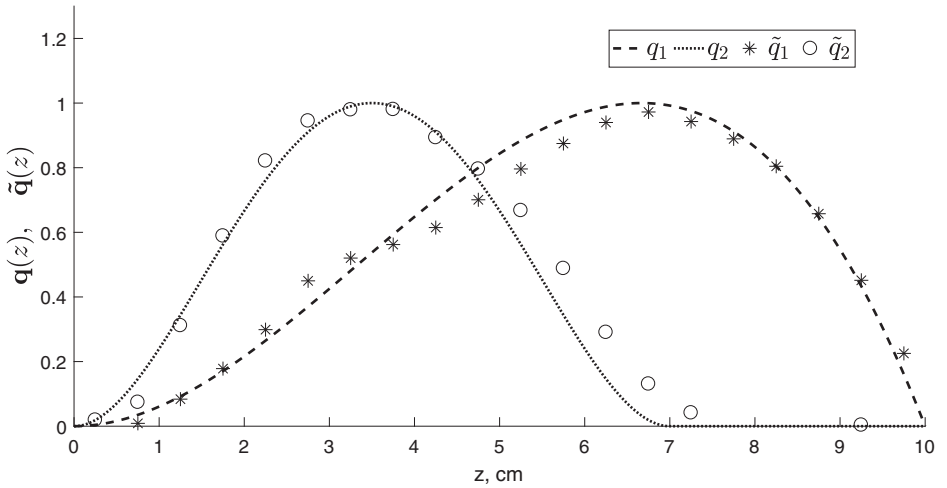

Figure 7. Components of exact and estimated sources using $\boldsymbol{W}_2$ to generate noisy measurements with Equation (40) and $B = 20$ in Equation (39). Lines represent exact component and asterisks estimated components.

5.2611%. The second energy group presented better results, 0.0941 of absolute error and 5.6370% of relative error.

However, using measurements with higher noise generated by the normal distribution with $\boldsymbol{W}_2$, we found much higher errors, as indicated in Figure 6. In fact, the absolute error was 0.2261 and the relative error was 10.9158% for the first energy group and, respectively, 0.2149 and 12.8681% of absolute and relative errors for the second group.

Proceeding, we keep the same physical parameters and exact source $\boldsymbol{q}$, however we increase the number of basis functions by setting $B = 20$ in Equation (39), and we keep the same readings displayed in Figure 4 generated using $\boldsymbol{W}_2$ in Equation (40). We plot, in Figure 7, the exact components of $\boldsymbol{q}$, and its estimated values.

We see in Figure 7 that the estimated components of $\boldsymbol{q}$ quite accurately approximate the exact components. In fact, we got an absolute error of 0.1585 for the first energy group, and 0.1990 for the second one, which led us to relative errors of 7.9164% and 11.8297%, respectively. Thus, we note that the errors (in Figure 7) were smaller than the ones obtained in Figure 6, in which case, for the same noisy reading, fewer basis functions were considered to approximate the source.

5.2. Test problem II

To provide a more challenging test problem, we consider a modified version of a six-group anisotropic problem related to neutron scattering in water (Siewert 1993b). The five matrices in (50) represent total cross-sectional (cm^{-1}) and group transfer data (cm^{-1}) of a homogeneous media

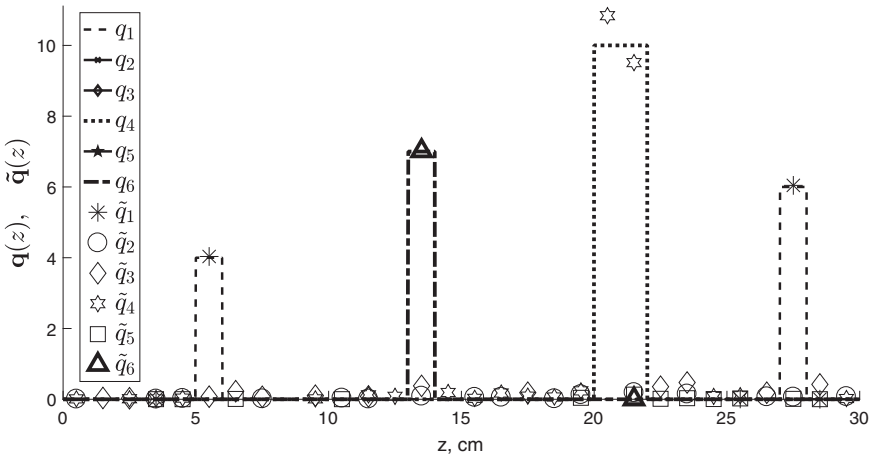

Figure 8. Components of the exact source and estimated source. Lines are used to represent the exact values of q_g, and markers to display the estimated values $\tilde{q}_g$, for $g = 1, \ldots, 6$.

problem defined for $z \in [0, 30]$ and anisotropy degree $L = 3$. We remark that, since we are considering an homogeneous media, we dropped the k index used to refer a specific region. We also denote $x \times 10^e$ as $x(+e)$, for any integer number e. Thus, we have

$$\boldsymbol{S} = \text{diag}(1.50520, 1.57051, 3.51907, 6.26226, 14.0294, 42.14920), \tag{50a}$$

$$\boldsymbol{T}_0 = \begin{bmatrix} 8.07750(-1) & 0.00000(+0) & 0.00000(+0) & 0.00000(+0) & 0.00000(+0) & 0.00000(+0) \\ 6.26456(-1) & 9.84040(-1) & 9.79447(-2) & 4.70592(-2) & 1.26378(-1) & 3.97098(-1) \\ 6.16969(-2) & 5.22489(-1) & 3.09892(+0) & 2.01540(+0) & 3.24243(+0) & 9.62747(+0) \\ 6.16969(-3) & 5.15850(-2) & 2.97524(-1) & 3.88257(+0) & 8.22842(+0) & 2.42148(+1) \\ 6.16969(-4) & 5.15850(-3) & 3.48269(-3) & 2.43839(-1) & 2.09399(+0) & 5.46759(+0) \\ 6.83147(-5) & 5.72919(-4) & 9.81407(-5) & 6.67680(-3) & 1.27601(-1) & 1.77484(+0) \end{bmatrix}, \tag{50b}$$

$$\boldsymbol{T}_1 = \begin{bmatrix} 1.73809(+0) & 0.00000(+0) & 0.00000(+0) & 0.00000(+0) & 0.00000(+0) & 0.00000(+0) \\ 1.00096(+0) & 2.06953(+0) & 3.65035(-2) & -7.17931(-3) & -6.57000(-3) & -6.21269(-3) \\ 3.23741(-2) & 7.97905(-1) & 1.84248(+0) & -8.37651(-1) & -9.50478(-1) & -8.87500(-1) \\ 1.16883(-3) & 2.58418(-2) & -1.42702(-2) & 1.51150(+0) & -1.42204(-1) & -5.72883(-1) \\ 8.28375(-5) & 9.49379(-4) & -1.60567(-3) & 7.80252(-2) & 1.18387(+0) & 1.21816(+0) \\ 2.28725(-5) & 9.04254(-5) & -1.63418(-5) & 3.64032(-4) & 2.94178(-2) & 5.93333(-1) \end{bmatrix}, \tag{50c}$$

$$\boldsymbol{T}_2 = \begin{bmatrix} 1.89361(+0) & 0.00000(+0) & 0.00000(+0) & 0.00000(+0) & 0.00000(+0) & 0.00000(+0) \\ -1.16776(-2) & 2.03360(+0) & -2.78866(-2) & -3.66853(-3) & -5.40201(-3) & -1.56529(-2) \\ -1.38579(-1) & -1.00130(-1) & 4.28177(-1) & -4.78174(-1) & -1.90615(-1) & -3.91507(-1) \\ -1.52290(-2) & -1.16769(-1) & -6.28730(-2) & 5.52373(-1) & -5.57599(-1) & -1.08378(+0) \\ -1.53296(-3) & -1.27412(-2) & -3.69913(-4) & 4.15341(-2) & 7.64138(-1) & 1.96411(-1) \\ -1.61574(-4) & -1.41761(-3) & -4.41786(-6) & -2.23975(-4) & 3.03330(-2) & 2.98538(-1) \end{bmatrix}, \tag{50d}$$

and

Table 2. Absolute and relative errors (L^2 norm) between the exact source q_g and the estimated $\tilde{q}_g$, for $g = 1, \ldots, 6$, using one reading by energy group for each basis function's support.

Energy group	1	2	3	4	5	6
Absolute error	0.0579	0.3319	0.9055	1.0577	0.1443	0.0166
Relative error	0.8025%	–	–	7.4791%	–	0.2371%

$$\boldsymbol{T}_3 = \begin{bmatrix} 1.28480(+0) & 0.00000(+0) & 0.00000(+0) & 0.00000(+0) & 0.00000(+0) & 0.00000(+0) \\ -1.17471(+0) & 1.09070(+0) & -2.12993(-2) & -7.43655(-4) & -5.91497(-4) & -5.66126(-4) \\ -1.05643(-1) & -1.00250(+0) & 4.61562(-1) & -1.88398(-1) & -8.54669(-2) & -7.69580(-2) \\ -4.05881(-3) & -8.45487(-2) & -2.85371(-2) & 7.24719(-1) & -1.03599(-2) & 6.50889(-2) \\ -2.88894(-4) & -3.29773(-3) & -1.53968(-4) & 5.10368(-2) & 7.61976(-1) & 2.89226(-1) \\ -7.47744(-5) & -3.13307(-4) & -1.46113(-6) & 5.06034(-5) & 3.23582(-2) & 2.85246(-1) \end{bmatrix}. \tag{50e}$$

In this case, we try to estimate an internal source of particles $\boldsymbol{q} = [q_1 q_2 q_3 q_4 q_5 q_6]^T$, whose components are

$$q_1(z) = \begin{cases} 4.0, & z \in [5.0, 6.0], \\ 6.0, & z \in [27.0, 28.0], \\ 0.0, & \text{otherwise}, \end{cases} \tag{51a}$$

$$q_4(z) = \begin{cases} 10.0, & z \in [20.0, 22.0], \\ 0.0, & \text{otherwise}, \end{cases} \tag{51b}$$

$$q_6(z) = \begin{cases} 7.0, & z \in [13.0, 14.0], \\ 0.0, & \text{otherwise}, \end{cases} \tag{51c}$$

and $q_g(z) = 0$, for $z \in [0, 30]$, with g = 2, 3, 5. As before, we consider vacuum boundary conditions,

$$\boldsymbol{\psi}(0, \mu) = \boldsymbol{0}, \tag{52a}$$

and

$$\boldsymbol{\psi}(30, -\mu) = \boldsymbol{0}, \tag{52b}$$

for $\mu \in [0, 1]$. For the estimation procedure, we use B = 30 in Equation (39) to generate basis functions. We use again the *Diamond Difference* method (Lewis and Miller 1984) to solve the transport problem (5) with N = 128, 100 nodes per *cm* and a tolerance of 10^{-12}, to generate exact measurements $\boldsymbol{r}_0$, and a covariance matrix $\boldsymbol{W}$, such that $\boldsymbol{W}^{1/2} = \text{diag}(0.01 \times \boldsymbol{r}_0)$. For our first test, we consider one reading in energy group for each basis function's support, and measurements with 0.0457 and 1.0060% of absolute and relative errors, respectively. We show, in Figure 8, graphs for the exact source (lines) and the values estimated using Equation (47) (markers).

As Figure 8 indicates, for the majority of the energy groups, we were able to recover the shape and magnitude of the exact source, except for a few discrepancies in group-4 and some minor oscillatory behavior near to

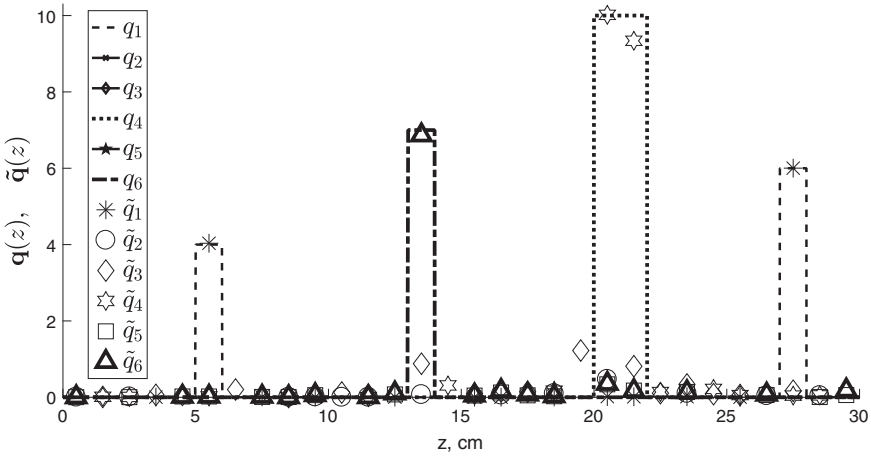

Figure 9. Components of the exact source and estimated source. Lines are used to represent the exact values of q_g, and markers to display the estimated values $\tilde{q}_g$, for $g = 1, \ldots, 6$. Two readings per group in each basis functions' support.

Table 3. Absolute and relative errors (L^2 norm) between the exact source q_g and the estimated $\tilde{q}_g$, for $g = 1, \ldots, 6$, using two reading by energy group for each basis function's support.

Energy group	1	2	3	4	5	6
Absolute error	0.0624	0.2724	0.9957	0.9295	0.3329	0.4745
Relative error	0.8658%	–	–	6.5726%	–	6.7790%

zero. Table 2 presents absolute and relative errors, in the L^2 norm, between the exact source q_g and the estimated $\tilde{q}_g$, for $g = 1, ..., 6$.

As indicated in Figure 8, the analysis of Table 2 confirms a larger error related to the reconstruction in the 4th energy group. We still note that we were not able to compute relative errors for all energy groups, due to the fact that the exact source is identically zero for $g = 2, 3, 5$.

Proceeding, we double the number of detectors, considering two readings by energy group in each basis function's support, and measurements with an absolute error of 0.0556, and relative error of 1.1651%. As before, in Figure 9 we plot the exact source (lines) and the values estimated using Equation (47) (markers).

Similarly to the previous case, Figure 9 points out that we were able to recover the shape and magnitude of the exact source, as well as have a closer estimate for the 4th energy group component of $\boldsymbol{q}$. However, we noticed the increase of the oscillatory behavior near zero.

An analysis of the results in Table 3 indicates that the error, for group-4, is now smaller. However, we see the error increased for the remaining groups, particularly for group-6. Despite of that, the maximum relative error among all groups has stayed below 6.8% (smaller than before).

We remark that we were able to perfectly estimate the exact source on both six-group tests when using error-free measurements. In addition, the regularization parameter used in Equation (47) was 10^{-7}, leading to worse estimations for either smaller or higher values.

To conclude this section, we emphasize that when calculating the matrix $\boldsymbol{A}$ in Equation (47), which is of order 360×180 in this final test, we were required to compute 64,800 inner products. Using numerical integration for the spatial variable, this process took roughly 30 minutes. However, using analytical expressions, as in Equation (30a), we were able to do the same in less than a minute.

6. Concluding remarks

We developed a fast, concise and accurate solution to the discrete ordinates approximation of the adjoint multigroup transport equation in slab geometry. Using that, and assuming sectionally constant absorption cross sections and basis functions, we were able to derive an explicit formula, Equation (30a), to evaluate the absorption rate of internal particle detectors. We found the approach very helpful to reduce computational time.

Two and six group problems were considered to test the formulation in source-detector problems type as well as in source estimation applications. In both cases numerical results obtained were very good in the sense of recovering shape and magnitude of the source from fast solutions.

For the case of source reconstruction problems, the usual sensitivity to noise added to the measurements, was noted. Surely the analysis can be extended to the use of different sets of basis functions, alternative regularization approaches or inverse problem solution techniques. In fact, since the search for non-negative solutions and the Tikhonov regularization used in this work add bias to our answer, we are investigating the application of Bayesian Inference methods.

It is also our idea, as future work, to improve the model by using nodal techniques to develop an ADO solution to adjoint multigroup transport problems in xy-geometry.

Acknowledgments

The authors would like to thank CNPq and CAPES for partial financial support to this work.

References

Badruzzaman, A. 1991. Computational methods in nuclear geophysics. *Progress Nuclear Energ.* 25 (2–3):265–290.

Barichello, L. B., and C. E. Siewert. 1999a. A discrete-ordinates solution for a non-grey model with complete frequency redistribution. *J. Quantitative Spec. Radiat. Transf.* 62 (6):665–675.

Barichello, L. B., and C. E. Siewert. 1999b. A discrete-ordinates solution for a polarization model with complete frequency redistribution. *APJ*. 513 (1):370–382.

Barros, R. C., and E. W. Larsen. 1991. A numerical method for multigroup slab-geometry discrete ordinates problems with no spatial truncation error. *Transp. Theor. Statistic Phys.* 20 (5–6):441–462.

Beck, J., and K. Arnold. 1977. *Parameter estimation in engineering and science*. New York, NY: John Wiley & Sons.

Bledsoe, K., and J. Favorite. 2007. Using the levenberg-marquardt method for the solution of inverse transport problems with scattering. American Nuclear Society, Proceedings of the Joint International Topical Meeting on Mathematics & Computations and Supercomputing in Nuclear Applications (M & C + SNA), Monterey, CA, April 15–19, pp. 1898–1912.

Dorn, O. 2000. Scattering and absorption transport sensitivity functions for optical tomography. *Opt. Express* 7 (13):492–506.

Duderstadt, J., and W. Martin. 1979. *Transport theory*. New York, NY: Wiley.

Gao, H., and H. Zhao. 2010. Multilevel bioluminescence tomography based on radiative transfer equation Part 1: L1 regularization. *Opt. Express* 18 (3):1854–1871.

Golub, G. H., and J. Welsch. 1969. Calculation of gauss quadrature rules. *Math. Comp*. 23 (106):221–230.

Haltmeier, M., L. Neumann, and S. Rabanser. 2015. Single-stage reconstruction algorithm for quantitative photoacoustic tomography. *Inverse Problem*. 31 (6):1–24.

Hykes, J., and Y. Y. Azmy. 2011. Radiation source reconstruction with known geometry and materials using the adjoint. Proceedings of the International Conference on Mathematics and Computational Methods Applied to Nuclear Science and Engineering (M&C), Rio de Janeiro, Brazil, May 8–12, pp. 1–15.

Kaipio, J., and E. Somersalo. 2005. *Statistical and computational inverse problems*. New York, NY: Springer.

Kauati, A., A. Silva Neto, and N. Roberty. 2001. A source-detector methodology for the construction and solution of the one-dimensional inverse transport equation. *Inverse Problem Eng.* 9 (1):45–66.

Lewis, E., and W. Miller. 1984. *Computational methods of neutron transport*. New York, NY: John Wiley & Sons.

Miller, K., and W. Charlton. 2007. An inverse transport approach to radiation source location for border security. Proceedings of the 29th Annual Meeting of the European Safeguards Research and Development Association, Aix-en-Provence, France, May 22–24.

Pazinatto, C. B., and L. B. Barichello. 2017. On the use of analytical techniques for source reconstruction problems. International Conference on Mathematics & Computational Methods Applied to Nuclear Science & Engineering, Jeju, Korea, April 16–20.

Pazinatto, C. B., R. C. Barros, and L. B. Barichello. 2016. Analytical adjoint discrete ordinates formulation for monoenergetic slab-geometry source-detector calculations. *IJNEST*. 10 (2):107–119.

Prinja, A., and E. Larsen. 2010. General principles of neutron transport, chapter 5. In *Handbook of nuclear engineering. Vol. 1 of Nuclear engineering fundamentals*. New York, NY: Springer.

Scherer, C., J. Prolo Filho, and L. Barichello. 2009. An analytical approach to the unified solution of kinetic equations in rarefied gas dynamics.I. flow problems. *Z. Angew. Math. Phys*. 60 (1):70–115.

Siewert, C. E. 1993a. An inverse source problem in radiative transfer. *J. Quantitat. Spectro. Rad. Transf*. 50 (6):603–609.

Siewert, C. E.1993b. A spherical-harmonics method for multi-group or non-gray radiation transport. *J. Quantitat. Spectro. Rad. Transf*. 49 (2):95–106.

Siewert, C. E. 2000. A discrete-ordinates solution for multigroup transport theory with upscattering. *J. Quantitat. Spectro. Rad. Transf*. 64:255–273.

Somasundaram, E., and T. Palmer. 2016. Application of variational variance reduction for source-detector problems in nuclear non-proliferation. *J. Comput. Theor. Transp*. 45 (7): 554–577.